Absolute calibration of the antiproton detection efficiency for BESS below 1 GeV with an accelerator beam test at KEK-PS

Y. Asaoka[1], **K. Yoshimura**[2], **T. Yoshida**[2], **K. Abe**[1], **K. Anraku**[1], **M. Fujikawa**[1], **H. Fuke**[1], **S. Haino**[1], **K. Izumi**[1], **T. Maeno**[3], **Y. Makida**[2], **N. Matsui**[1], **H. Matsumoto**[1], **H. Matsunaga**[1, †], **M. Motoki**[1, ‡], **M. Nozaki**[3], **S. Orito**[1, *], **T. Sanuki**[1], **M. Sasaki**[2], **Y. Shikaze**[1], **T. Sonoda**[1], **J. Suzuki**[2], **K. Tanaka**[2], **Y. Toki**[3], and **A. Yamamoto**[2]

[1]The University of Tokyo, Tokyo, 113–0033 JAPAN
[2]High Energy Accelerator Research Organization (KEK), Tsukuba, Ibaraki 305–0801, JAPAN
[3]Kobe University, Kobe, Hyogo, 657–8501 JAPAN

Abstract. An accelerator beam test was performed using a low-energy antiproton beam to measure the antiproton detection efficiency of the BESS detector. Measured and calculated efficiencies derived from the BESS Monte Carlo simulation based on GEANT/GHEISHA showed good agreement. With the detailed verification of the BESS simulation, results demonstrate that the relative systematic error in detection efficiency derived from the BESS simulation is within $\pm$ 5%, being previously estimated as $\pm$ 15% which was the dominant uncertainty for measurements of cosmic-ray antiproton flux.

1 Introduction

The BESS spectrometer, shown in Fig. 1, was designed (Orito et al., 1987; Yamamoto et al., 1988) and constructed (Yamamoto et al., 1994; Ajima et al., 2000) as a high-resolution spectrometer with the capability to search for rare cosmic-rays and provide various precision measurements of cosmic-ray primaries. A uniform magnetic field of 1 Tesla is produced by a thin superconducting coil (Makida et al., 1995), with substantial incident particles passing through without interaction. The magnetic-field region is filled with a tracking detectors composed of a jet type drift chamber (JET) and inner drift chambers (IDCs). Tracking is performed by fitting up to 28 hit-points in the drift chambers. Energy deposit in the drift chamber gas is also obtained as a truncated mean of the integrated charges of hit pulses. The upper and lower scintillator-hodoscopes (TOF) (Shikaze et al., 2000) provide two dE/dx measurements and the time-of-flight of particles. The instrument also incorporates a threshold-type Cherenkov counter (Asaoka et al., 1998) with a silica-aerogel radiator.

Correspondence to: Y. Asaoka
(asaoka@icepp.s.u-tokyo.ac.jp)

† Currently at Univ. of Tsukuba, Tsukuba, Ibaraki 305-8571, Japan
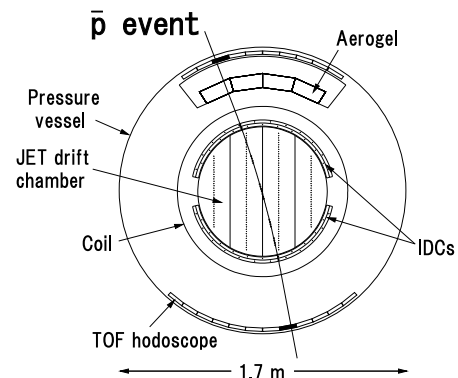‡ Currently at Tohoku University, Sendai, Miyagi 980-8578, Japan
* deceased

Fig. 1. Cross-sectional view of the BESS detector showing a $\bar{p}$ event.

Here, cylindrical coordinates (r, ϕ, and z) and Cartesian coordinates (x, y, and z) are used for representing the BESS instrument, where y and z are respectively the vertical axis and axis of the solenoid.

Since 1993, seven balloon flights have been successfully carried out and more than 10^3 antiprotons ($\bar{p}$'s) have been unambiguously detected. This has allowed measuring the energy spectrum of cosmic $\bar{p}$'s and investigating the origin of them.

To investigate the origin of low energy $\bar{p}$'s more sensitively, it is inevitable to reduce systematic errors as well as statistical errors of the resultant spectrum in the low energy region. The dominant source of systematic error in the low energy region ($<$ 1GeV) is uncertainty in the $\bar{p}$ interaction losses in the instrument. For the BESS detector we surmised $\pm$15 % relative error to the detection efficiency which is evaluated using the Monte Carlo simulation (BESS MC) (Matsunaga et al., 1997) based on the GEANT/GHEISHA code (Brun et al., 1994; Fesefeldt et al., 1985). The BESS MC incorporates detailed material and detector descriptions such that realistic detector performance is obtained. The original GHEISHA code was modified so that experimental data of $\bar{p}$-nuclei cross sections are reproduced. However, it is hard to

estimate the systematic error due to interaction losses in the instrument because of uncertainties in secondary multiplicity, angular distribution and detector response. Therefore, the detection efficiency must be directly measured and be precisely verified to reduce systematic error of the $\bar{p}$ flux.

Considering this, an accelerator beam test of the BESS detector was performed at KEK-PS K2 beam line using low energy $\bar{p}$ and proton beam. The main objectives of the beam test are as follows. (1) Direct measurement of detection efficiencies for $\bar{p}$'s and protons; (2) tests of the BESS MC simulation; (3) reducing the systematic error of the detection efficiency for $\bar{p}$'s. Simultaneous measurement of detection efficiencies for $\bar{p}$'s and protons helps to achieve (2) and (3) because they behave similarly in the instrument except for deflection in the magnetic field and inelastic interactions.

2 Detection Efficiency

The detection efficiency (ε) of $\bar{p}$'s (protons) is defined as:

$$\varepsilon = \frac{N_{\mathrm{obs}}}{N_{\mathrm{inc}}},$$

where N_{inc} is the number of incident $\bar{p}$'s (protons) within the acceptance of the detector, and N_{obs} is the number of particles identified as $\bar{p}$'s (protons). Owing to the symmetrical detector configuration of the BESS instrument, the non-interacting antiproton behave like a proton except for deflection. Therefore we applied the same selection criteria as protons for $\bar{p}$ identification (Maeno et al., 2001). In flight data, protons can be obtained with sufficient statistics by utilizing unbiased samples since they are the most abundant species in cosmic radiation. In the analysis of flight data, interaction losses are estimated using the BESS MC, while other efficiencies can be precisely estimated by proton samples. The detection efficiency can be decomposed into two factors.

$$\varepsilon = \varepsilon_{\mathrm{non-int}} \cdot \varepsilon_{\mathrm{ID}},$$

where $\varepsilon_{\mathrm{non-int}}$ is the non-interacting efficiency defined by single particle selection, fiducial volume cut and dE/dx band cuts in upper and lower TOF hodoscopes, and $\varepsilon_{\mathrm{ID}}$ is the identification efficiency defined by track quality cut and particle identification by using reconstructed mass and JET dE/dx. Since $\varepsilon_{\mathrm{ID}}(\bar{p}) = \varepsilon_{\mathrm{ID}}(p)$, the detection efficiency can be expressed as:

$$\varepsilon(\bar{p}) = \varepsilon_{\mathrm{non-int}}(\bar{p}) \cdot \varepsilon_{\mathrm{ID}}(\bar{p}) = \varepsilon_{\mathrm{non-int}}(\bar{p}) \cdot \varepsilon_{\mathrm{ID}}(p).$$

Considering the above equations, since $\varepsilon_{\mathrm{ID}}(p)$ can be precisely estimated using flight data, the total systematic error in $\varepsilon(\bar{p})$ can be reduced if we evaluate $\varepsilon_{\mathrm{non-int}}(\bar{p})$ using the beam test data.

3 Experimental Setup

The BESS beam test was performed in February 1999 at the KEK-PS K2 beam line which is equipped with an electrostatic separator (Yamamoto et al., 1982) to enrich low energy

kaons and $\bar{p}$'s. The BESS detector was located 8 m downstream of the focal point because the other experiment was being run in parallel. The resultant beam profile at the detector was about 20 cm (W) × 10 cm (H), being a beam spread in which detector performance is uniform. Figure 2 shows a schematic view of the experimental setup at the down stream of the K2 beam line. D2 is a dipole magnet, Q6 and Q7 are quadrapole magnets. They are used for beam transport and focusing. KURAMA is another dipole magnet to analyze momentum of the incident particles. The BESS detector was rotated circumferentially 70° in $r - \phi$ plane in the beam line for proper beam incidence.
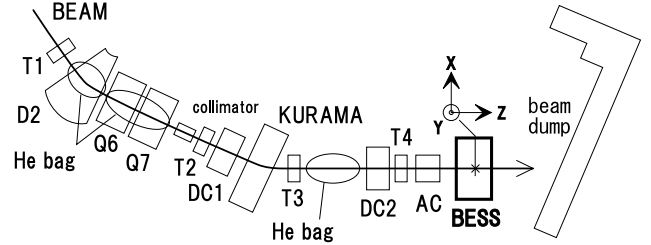

Fig. 2. Experimental setup at the downstream of K2 beam area for the BESS beam test.

Since there were more than 3 g/cm^2 materials left in the K2 beam line other than our detectors, interaction and energy losses of incident particles cannot be neglected. To reject interacted events and to identify incident particles, we placed 4 trigger counters (T1–T4), 2 drift chambers(DC1, DC2), and an aerogel Cherenkov counter(AC) in the beam line. In what follows, a right-handed coordinate system, with the z-axis along the beam direction, the y-axis vertical and upwards, and the origin at the center of the BESS detector position is used for the beam line. The position of each detector is also sketched in Fig. 2. Specifications of these detectors are summarized in Table 1.

Table 1. Summary of beam line instrumentation.

Detector Name	Location (m)	Resolution	
T1	−15.000	30	(ps)
T2	−8.000	30	
T3	−5.000	30	
NORMAL T4	−2.250	30	
WIDE T4	−2.250	40	
DC1	−7.853	150	(μm)
DC2	−2.296	150	
AC	−1.971	$> 10^4$	(rej. factor)
BESS	0.000	—	

Since the BESS detector exhibits uniform performance over a wide region due to the simple cylindrical geometry and uniform magnetic field, there is no need to perform a detailed position/angle scan of detection efficiency. Data was collected for three different detector configurations. Each configuration, i.e., CFG1, CFG2, and CFG3, is shown in Fig. 3. As these configurations were selected to represent the incidence

of cosmic-ray particles in terms of the amount of material and penetrated region, a total test of the BESS MC can be performed by combining the data from the three configurations.
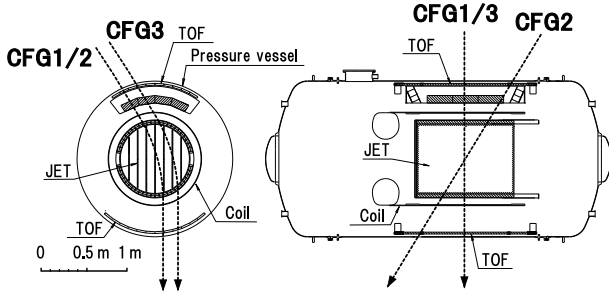

Fig. 3. Cross sectional view of BESS detector with incident $\bar{p}$ beam for each configuration(CFG1–3). Using CFG1 as a reference, CFG2 was the case that incident beam has an angle of $\cos\theta = 0.915$, where θ is defined as the angle between beam and y-axis in the y-z plane. CFG3 was the case that the incident beam passed through different region of central tracking system in the $r - \phi$ plane. The distance of incident position between CFG1 and CFG3 was 15.3 cm along the x-axis.

The kinetic energy of incident particles at the BESS top of instrument (E_{TOI}) ranges from 0.1 to 1 GeV (0.4 to 1 GeV) for $\bar{p}$'s (protons). The BESS detector cannot be rotated more than 70 ° due to a constraint in the liquid helium storage, and therefore low energy protons were out of the BESS acceptance region in this beam test.

4 Beam identification

To determine N_{inc} the beam line detectors must clearly identify the incident particle and precisely determine their incident position, angle, and energy. In order to select $\bar{p}$ and proton events, the following cuts were applied on the beam test data set. (1) a good beam track should exist in the beam line detector DC1 and DC2; (2) the incident particle must have proper deflection angle at KURAMA; (3) dE/dx in T1, T2, T3 and T4 should be compatible with $\bar{p}$'s; (4) $1/\beta$ between T2−T1, T3−T1, T4−T1, T3−T2, T4−T2 and T4−T3 are consistent to that of $\bar{p}$'s; (5) light particles are rejected by veto of AC light output (Q_{AC}). These cuts combined are referred to as BID0. The most effective cuts are $1/\beta_{T4-T3}$ and dE/dx_{T4} cut. Q_{AC} veto is also important because it rejects a part of interacted events in T4 and AC itself. Examples for BID0 for $\bar{p}$'s of $E_{TOI} \sim 1$ GeV are shown in Fig. 4. Since the $1/\beta$ distribution shows the clear separation between $\bar{p}$, kaon, and pion/muon/electron, the incident beam particles are unambiguously identified.

In order to compare the beam data and BESS MC results, a MC data set was generated as follows. To estimate interaction and energy losses in T4 and AC, which were located just upstream of BESS, they were included in the simulation. Input kinematics of beam particles was obtained by beam data event by event; i.e., the incident position and angle were
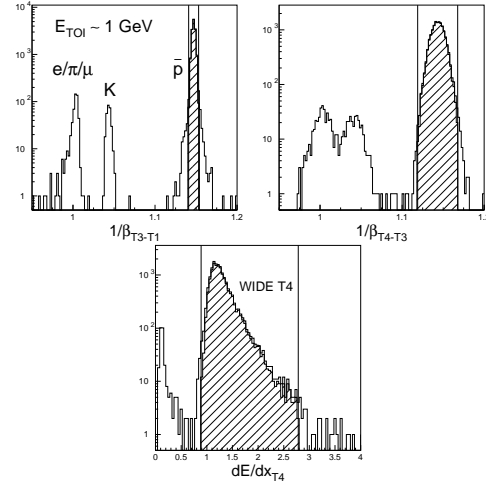

Fig. 4. $1/\beta$ and dE/dx cut by trigger counters for $\bar{p}$'s of $E_{TOI} \sim 1$ GeV. $1/\beta_{T3-T1}$, $1/\beta_{T4-T3}$ and dE/dx_{T4} are shown in (a), (b) and (c), respectively. The hatched histogram means survived events after applying BID0.

determined by beam track, while the incident energy was determined by $1/\beta_{T4-T3}$. This allows comparisons between beam data and MC results under the same conditions. Data sets are referred to as BEAM and MC, respectively.

Although the beam identification was performed by BID0, we found that the contamination on N_{inc} caused by interaction and/or scattering of incident particles after DC2 was not negligible. We need to be assured that the incident particle arrives at the BESS top of instrument by adding cuts to BID0. Information from upper TOF hodoscope is used for this purpose. we should use this information carefully not to reject interacted events in the BESS instrument.

In addition to BID0, the following cuts were applied: (6) Number of hits in upper TOF hodoscope should be greater than 0; (7) require beam trajectory agreement with upper TOF hit position in both $r-\phi$ and $y-z$ plane, which are hereafter referred to as BID1. Note that BID1 includes BID0. BID1 guaranteed that the incident particle passes through T4 and AC without large angle scattering or interaction. A percentage that BID1 rejected events which interacted in the BESS instrument was kept low enough, at most 1% (estimated by the BESS MC), thus we can conclude that BID1 completely remove the effect of T4 and AC, resulting in the exact determination of N_{inc}.

5 Result

Figure 5 shows the non-interacting efficiency for $\bar{p}$'s and protons derived from BEAM together with that derived from MC for each configuration.

They are in good agreement with each other. The error bars of each data point include both statistical and systematic uncertainties. Possible sources of beam related systematic errors are (1) beam dump effect, (2) accidental track identification and (3) beam identification using the upper TOF.
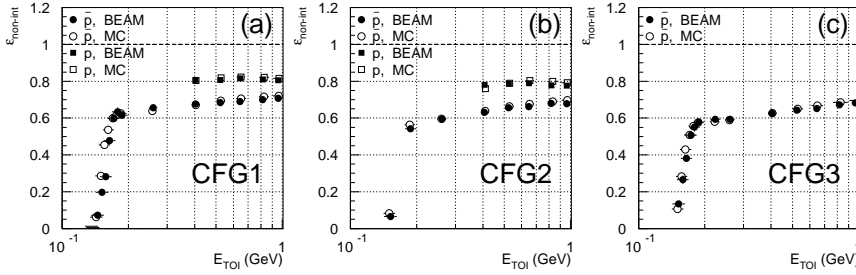
Fig. 5. The direct measurement of the non-interacting efficiency for $\bar{p}$'s(circles) and protons(squares) in CFG1(a), CFG2(b) and CFG3(c). Close and open symbols represent BEAM and MC, respectively.

They were studied in detail and carefully estimated (Asaoka et al., 2001). Moreover, to understand the BESS MC, intensive studies were performed on the amount of material, secondary multiplicity, angular distribution, cross section and detector response (Asaoka et al., 2001).

At last, the systematic error in detection efficiency over the whole BESS fiducial was evaluated. Since efficiencies are averaged over the whole acceptance region in the flight data analysis, we combined the data of three configurations, i.e., CFG1–3. The difference in the combined non-interacting efficiency between BEAM and MC ($(\Delta\varepsilon/\varepsilon)_{\mathrm{non-int}} \equiv (\varepsilon_{\mathrm{MC}} - \varepsilon_{\mathrm{beam}})/\varepsilon_{\mathrm{beam}}$) are shown in Fig. 6 for (a) $\bar{p}$'s and (b) protons (represented by closed circles). Note that the error bars of each data points in Fig. 6 include the maximum deviation of the efficiency difference between all configurations in addition to beam related systematic errors. As shown, the
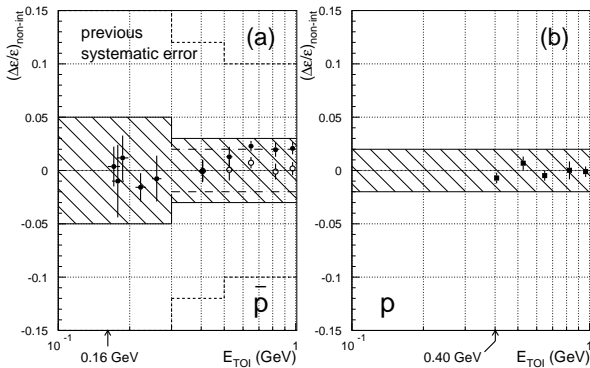

Fig. 6. Test of the non-interacting efficiency derived from the BESS MC for (a) $\bar{p}$'s and (b) protons. Close symbols represent the relative differences between BEAM and MC combining all CFG's. Dotted line in (a) is the previous systematic error surmised to the detection efficiency.

accelerator beam calibration confirmed that the BESS MC gave reasonably correct detection efficiencies, and reduced the systematic error in detection efficiency for $\bar{p}$'s to within 5 and 3% from 0.16 to 0.3 and 0.3 to 1.0 GeV, respectively; and for protons to within 2% from 0.4 to 1.0 GeV (represented by hatched area). In addition, the use of further tuned MC with modified cross section (Asaoka et al., 2001) reproduces detection efficiency exactly and the systematic error in detection efficiency can be reduced to $\pm$ 2% from 0.3 to 1 GeV for $\bar{p}$'s (represented by open circles).

6   Summary and Conclusion

Using an accelerator beam experiment, the absolute calibration of the detection efficiency for $\bar{p}$'s and protons was performed below 1 GeV, with the BESS Monte Carlo simulation being verified in detail as well. The calibration remarkably reduced the relative systematic error in detection efficiency derived from the simulation, especially for $\bar{p}$'s which can be applied to systematic errors in cosmic-ray $\bar{p}$ measurements (Matsunaga et al., 1998; Orito et al., 2000; Maeno et al., 2001), as well as forthcoming data from 1999/2000 flights (Asaoka and Ormes et al., 2001) and future BESS experiments including high statistics long-duration flights (Yamamoto and Mitchell et al., 2001) providing the instrumental features of BESS are maintained. By increasing the reliability of the cosmic-ray $\bar{p}$ spectrum, these results will enable us to carry out the most sensitive-ever investigation on the origin of cosmic-ray $\bar{p}$'s.

References

Ajima, Y., et al., 2000, *Nucl. Instrum. Methods A 443*, 71.

Asaoka, Y., et al., 1998, *Nucl. Instrum. Methods A 416*, 236.

Asaoka, Y., et al., 2001, physics/0105003, submitted to *Nucl. Instrm. Methods A*.

Asaoka, Y. and Ormes, J., et al., 2001, This conference, *27th ICRC (Hamburg)*.

Brun, R., et al.., 1994, GEANT3.21, *CERN Program Library Long Write up W5013*.

Fesefeldt, H., 1985, *PITHA 85/02, Aachen*.

Maeno, T., et al., 2001, *Astropart. Phys.*, in press.

Makida, Y. et al., 1995, *IEEE Trans. Applied Supercon. 5(2)*, 638.

Matsunaga, H., 1997, *Ph.D. thesis*, University of Tokyo.

Matsunaga, H., et al., 1998, *Phys. Rev. Lett. 81*, 4052.

Orito, S., 1987, *ASTROMAG Workshop, KEK Report 87-19*, 111.

Orito, S., et al., 2000, *Phys. Rev. Lett. 84*, 1078.

Shikaze, Y., et al., 2000, *Nucl. Instrum. Methods A 455*, 596.

Yamamoto, A., et al., 1982, *Nucl. Instrum. Methods A 203*, 35.

Yamamoto, A., et al., 1988, *IEEE Trans. Magn. 24*, 1421.

Yamamoto, A., et al., 1994, *Adv. Space Res. 14(2)*, 75.

Yamamoto, A., Mitchell, J., et al., 2001, This conference, *27th ICRC (Hamburg)*.